Hindawi
Geofluids
Volume 2022, Article ID 2284648, 15 pages
https://doi.org/10.1155/2022/2284648

Research Article

Anisotropic Hypoplastic Model Considering the Relation between Fabric Tensor and Anisotropic Parameters

Yong-Gwang Jong,[1,2] **Zixuan Chen**,[1] **YongMin Ma**,[1,3] **and Yang Liu**[1]

[1]*School of Civil & Resource Engineering, University of Science and Technology Beijing, Beijing 100083, China*
[2]*School of Material Engineering, Kim Chaek University of Technology, Pyongyang 999093, Democratic People's Republic of Korea*
[3]*School of Resource Prospecting Engineering, Kim Chaek University of Technology, Pyongyang 999093, Democratic People's Republic of Korea*

Correspondence should be addressed to Yang Liu; yangliu@ustb.edu.cn

Received 16 March 2022; Revised 15 September 2022; Accepted 21 September 2022; Published 15 October 2022

Academic Editor: Xianwei Zhang

The fabric anisotropy and anisotropic parameters have great effect on the mechanical property of sand. Based on the existing anisotropic model, a modified anisotropic hypoplastic model is developed by incorporating the relation between fabric tensor and anisotropic parameters into the nonlinear part of the constitutive model. The applicability of the improved anisotropic hypoplastic model is validated by comparing with the existing model and experimental data. As a result, it is found that the modified model can well predict the mechanical response of anisotropic sand.

1. Introduction

Natural sands are affected by gravity and other factors during deposition, which form a certain spatial arrangement among the particles. This progress causes the anisotropy of sand. The study on the anisotropic sand has always been an important research topic in the field of mechanics, which is of great significance for the analysis of deformation, mechanical properties, and stability of engineering rock and soil.

Numerous anisotropic plastic models and damage models have been used to predict the mechanical response of anisotropic soil and rock [1–6]. Based on the framework of critical state soil mechanics (CSSM) for the triaxial space, Dafalias et al. [1] have presented an anisotropic clay plasticity constitutive model. This new model was extended to include a non-associative flow rule and used to simulate the response under undrained loading for some normally consolidated sensitive clays, including possible softening response. An anisotropic elastoplastic model for soft clays has been established by Sivasithamparam and Castro [4] based on an existing model called S-CLAY1S, which is a Cam clay type model that accounts for anisotropy and destructuration. Rong et al. [6] have developed a statistical damage constitutive model for anisotropic rock and accurately predicted the mechanical state and deformation of rock for geotechnical, coal mining, shale gas exploitation, etc. However, these models are described by complex formulation and parameters. Meanwhile, traditional elastoplastic theories such as flow rule, destruction rule, and hardening rule have to be taken into account, and many assumptions must be selected.

Therefore, many researchers have paid special attention to develop hypoplastic models [7–27]. The hypoplastic models do not need to consider the traditional plastic theory and are developed without separating the deformation into the elastic and plastic parts, and only a simple formula can describe the complex constitutive relationship. A hypoplastic constitutive model has been first developed by Kolymbas [7], who used a simple nonlinear tensor equation to simulate the mechanical responses of sand. The equation is mainly divided into two parts: the first part is a linear function of the strain rate, the second part is a nonlinear function of the strain rate, and the stress rate tensor is represented by

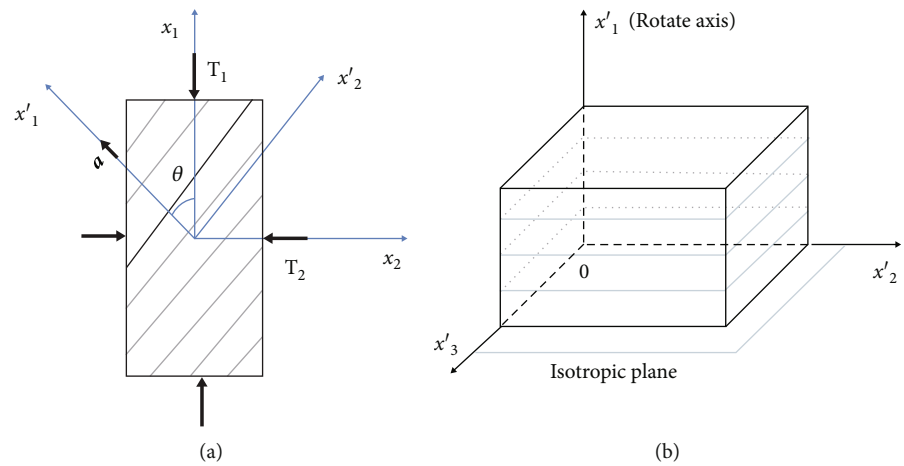

Figure 1: Coordinate system (a) and isotropic plane (b) of transverse isotropic sand.

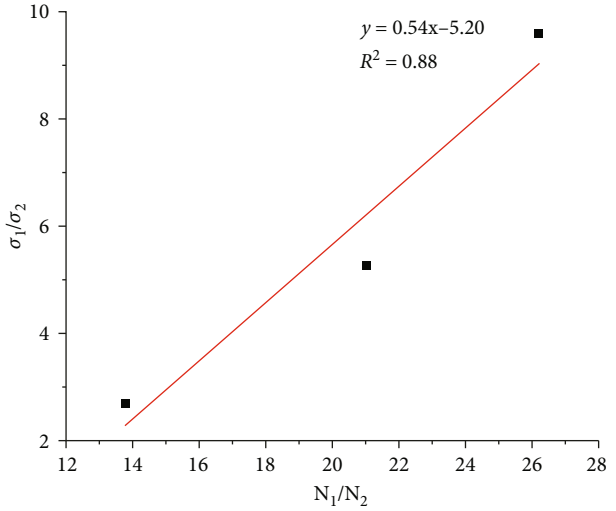

Figure 2: Stress ratio-anisotropy index curve ($\theta = 0^\circ$) ($^*N_1/N_2$ is an anisotropy index related to the distribution of contact normal. N_1 and N_2 are the maximum and minimum densities of contact normal, respectively.)

these two parts. A four-parameter hypoplastic model (called Wu-Bauer hypoplastic model) has been presented by Wu and Bauer [8] in 1994, and this constitutive relation was used to predict nonlinear stress-strain relationship and volume change in dilation of sand. The model requires four material parameters, which are simple to identify from triaxial compression tests. Since the model does not consider the concept of critical state, so it cannot reflect the descending part after the peak in the stress-strain relationship and describe the strain softening characteristics of dense sand. These limitations have been addressed in the later versions of models presented by previous studies [9–12], in which the void ratio was considered as an additional state variable to solve the above shortcomings. A hypoplastic damage model was developed from the fundamental concepts of hypoplastic theory and the damage state function by Zhang et al. [13]. Comparison of the predictions with the experimental results shows that the model can describe the main behavior of coarse grained soils, including the nonlinear relationship between the strength and the confining pressure and the volumetric strain behavior which dilates with low confining pressures but contracts with higher confining pressures. Recently, a new hypoplastic constitutive model has been presented by adopting a so-called intergranular strain and used to eliminate ratcheting under cyclic load [14, 15]. Liu et al. [19] have established a simple hypoplastic model to represent the mechanical responses of methane hydrate-bearing sands (MHBS). This new model was introduced with a new state parameter that considers the coupled effects of temperature and pore pressure on the mechanical behaviors of MHBS. Based on a basic hypoplastic model developed recently for sand, Wang et al. [26] have presented a new rate-dependent hypoplastic constitutive model for overconsolidated clays. The improved model was introduced with new density and stiffness factors adopted by considering history dependence. In addition, the new model was established by incorporating the Matsuoka-Nakai failure surface for the limit stress criterion. The model can properly predict the hardening/softening, shear dilation/contraction, and asymptotic state for overconsolidated clays.

Further, many researchers have developed anisotropic hypoplastic models to simulate the mechanical response of anisotropic soil based on the above hypoplastic models [28–44]. On the basis of the consideration of the principle of objectivity and the condition of material symmetry, Wu [28] has developed a new hypoplastic model for inherently anisotropic sand by incorporating a vector normal to the bedding plane into the explicitly granular hypoplastic models, which reproduces the mechanical behaviors of anisotropic sand. Bauer et al. [30] considered the evolution of anisotropy with the relative density of sand and assumed that the influence of the initial anisotropy diminished gradually, and it was completely gone at the critical state. An inherently isotropic hypoplastic constitutive model has been

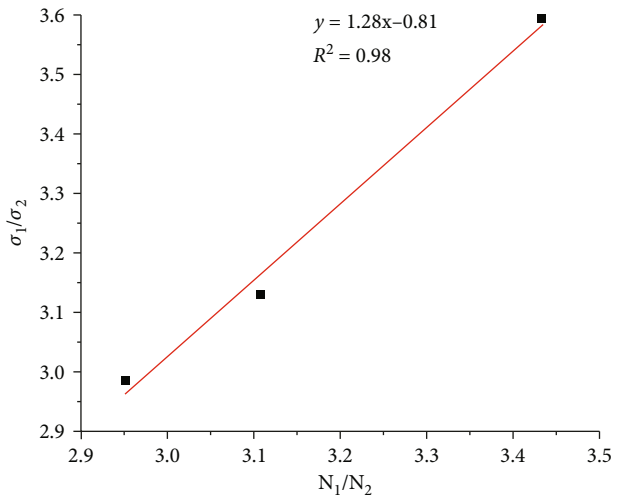

Figure 3: Stress ratio-anisotropy index curve (θ =60°) ($*N_1/N_2$ is an anisotropy index related to the distribution of contact normal. N_1 and N_2 are the maximum and minimum densities of contact normal, respectively.)

Table 1: Parameters for the evaluation of anisotropic hypoplastic model (Karlsruhe sand) [8, 47].

Parameters	Value	Parameters	Value
c_1	-101.2	α	1 (initial value)
c_2	-962.1	β	1 (initial value)
c_3	-877.3	γ	1 (initial value)
c_4	1229.2	χ	0.01, 0.02, 0.03

extended to the anisotropic hypoplastic model [32]. The modified model was developed by applying an anisotropy operator to the nonlinear part and the whole part of the existing hypoplastic model. The anisotropy operator includes two factors: vector a and anisotropic coefficients (α, β, γ). Vector a defines the orientation of the bedding plane, while the parameters (α, β, γ) show the degree of anisotropy. A new anisotropic hypoplastic model with fabric anisotropy has been presented by Herrera and Lizcano [35]. Because fabric tensors can affect the constitutive equations of sands by describing different granular material responses when subjected to different stress paths, so the new model is capable of predicting the mechanical behavior of the anisotropic sand. Mašín [36] has extended an anisotropic hypoplastic model to clay. The new model was developed by incorporating an anisotropic form of the stiffness tensor into the existing hypoplastic model with the asymptotic state boundary surface. By comparing simulation results with hollow cylinder apparatus experimental data, it has been proven that the model can be used for modeling the anisotropy influence on undrained stress paths. Recently, the anisotropic critical state theory (ACST) has been introduced into the hypoplastic model and used to simulate the anisotropic response of the soil. Yang et al. [39] have proposed a modified hypoplastic model for granular soils within the newly developed ACST. A deviatoric fabric tensor and a scalar-valued anisotropic state variable were incorporated into the modified model to simulate the effect of anisotropic fabric on the mechanical property of the anisotropic soil. Based on the ACST, Liao and Yang [41] have developed a unified hypoplastic model to reproduce the fabric effect in sand under both cyclic and monotonic loading conditions. The new model was introduced with the intergranular strain concept and an evolving deviatoric fabric tensor. A scalar-valued fabric anisotropic variable indicated the interaction between the fabric and the loading direction and was used to represent the effect of fabric anisotropy on both the dilatancy and shear strength of sand. Meanwhile, Liao and Yang [42] have adopted the ACST framework and presented an extended hypoplastic model to predict the noncoaxial and anisotropic response of sand subjected to both rotation of principal stress axis and monotonic loading. Based on the fabric change effect and a new unloading criterion, Liao and Yang [43] have developed an enhanced hypoplastic model to realistically predict soil behaviors under multidirectional shearing conditions. By comparing the simulation results of four models, including anisotropic hypoplastic model, with experimental results, Duque et al. [44] have investigated the advantages and disadvantages of these constitutive models for anisotropic fine-grained soils.

Based on the existing anisotropic hypoplastic model, in this paper, a new improved model has been proposed by considering evolution of the fabric and anisotropic parameters under the external loading. Previous works assumed that the coefficients of anisotropy are constant, and the evolution of anisotropy depends on the relative density. The modified model is introduced by incorporating the relation between the fabric tensor and anisotropic parameters into the nonlinear part of the constitutive model. According to one viewpoint (the relation between fabric tensor and anisotropic parameters) described above, this paper has the originality that is different from the previous papers.

2. A New Improved Model

2.1. Existing Anisotropic Hypoplastic Model. Based on the anisotropic hypoplastic model proposed by Wu [28], and Osinov and Wu [32], a new improved model has been developed. It uses a constitutive formulation expressed as

$$\dot{\mathbf{T}} = \mathbf{L}(\mathbf{T}) : \mathbf{D} + \mathbf{M}(\mathbf{A}, \mathbf{N}) \|\mathbf{D}\|, \tag{1}$$

where $\dot{\mathbf{T}}$ is the material time derivative of the stress tensor $\mathbf{T}$, and $\mathbf{D}$ is the rate of deformation tensor. $\mathbf{L}(\mathbf{T})$ and $\mathbf{N}$ are the fourth-order tensor and the second-order tensor, respectively. $\|\mathbf{D}\| = \sqrt{\mathrm{tr}(\mathbf{DD})}$ stands for a norm. $\mathbf{M}$ is the function of the tensors $\mathbf{A}$ and $\mathbf{N}$. The tensor $\mathbf{A}$ can be written as follows:

$$\mathbf{A} = \boldsymbol{a} \otimes \boldsymbol{a} = \begin{bmatrix} +\cos\theta\cos\theta & -\sin\theta\cos\theta & 0 \\ -\sin\theta\cos\theta & +\sin\theta\sin\theta & 0 \\ 0 & 0 & 0 \end{bmatrix}, \tag{2}$$

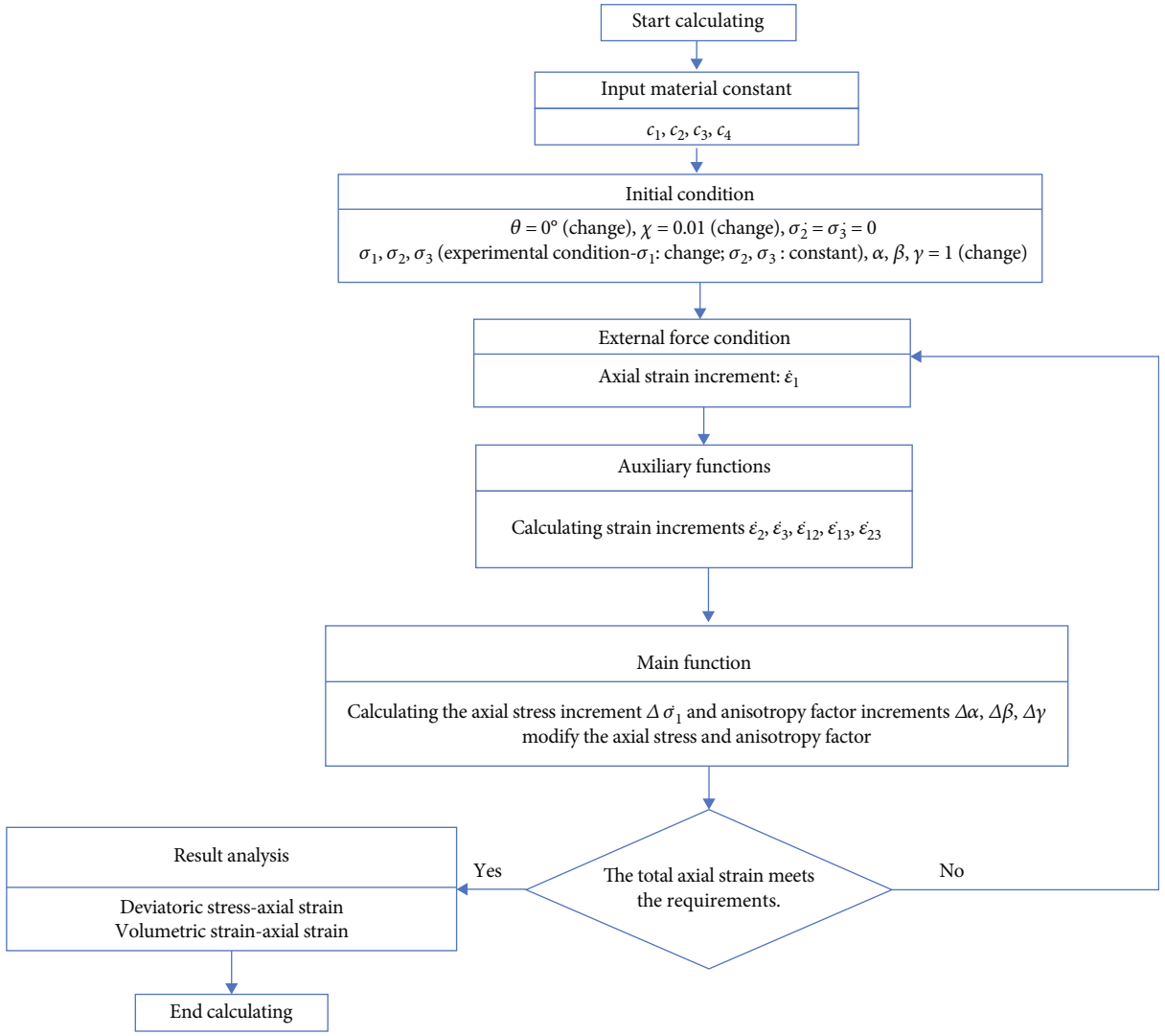

Figure 4: Operation flow of the MATLAB code.

where a is a vector, and θ is the bedding angle. Figure 1 shows the coordinate system and isotropic plane of transverse isotropic sand. Based on a Cartesian coordinate system (x_1, x_2) in which the axis x_1 is aligned with the major principal stress, assuming a new rotated system (x_1', x_2') in which the axis x_1' coincides with the direction of the transverse isotropy determined by the vector a. θ is the angle between x_1 and x_1'.

Based on Euler's theorem for homogeneous functions, they assumed that the definition of $\mathbf{M}$ is as follows:

$$\mathbf{M}(\mathbf{A}, \mathbf{N}) = \mathbf{B}(\mathbf{A})\mathbf{N}, \tag{3}$$

where the fourth-order tensor $\mathbf{B}(\mathbf{A})$ is a function of $\mathbf{A}$ and is independent of $\mathbf{N}$. Since both $\mathbf{M}$ and $\mathbf{N}$ are symmetric tensors of the second-order, $\mathbf{B}$ and $\mathbf{N}$ are represented with matrices of 6×6 and 6×1, respectively, and Equation (3) can be rewritten as follows:

$$\{\mathbf{M}\} = [\mathbf{B}]\{\mathbf{N}\} = \begin{bmatrix} b_{11} & b_{12} & b_{12} & 0 & 0 & 0 \\ b_{12} & b_{22} & b_{23} & 0 & 0 & 0 \\ b_{12} & b_{23} & b_{22} & 0 & 0 & 0 \\ 0 & 0 & 0 & b_{44} & 0 & 0 \\ 0 & 0 & 0 & 0 & b_{44} & 0 \\ 0 & 0 & 0 & 0 & 0 & b_{22} - b_{23} \end{bmatrix} \begin{bmatrix} N_{11} \\ N_{22} \\ N_{33} \\ N_{23} \\ N_{13} \\ N_{12} \end{bmatrix}. \tag{4}$$

The elements in matrix $[\mathbf{B}]$ are the so-called anisotropic parameters to be determined. For the purpose of simplification, the off-diagonal elements in Equation (4) were eliminated, and three coefficients ($b_{11} = \alpha$, $b_{22} = \beta$, and $b_{44} = \gamma$) were retained. Thus, Equation (4) can be redefined as

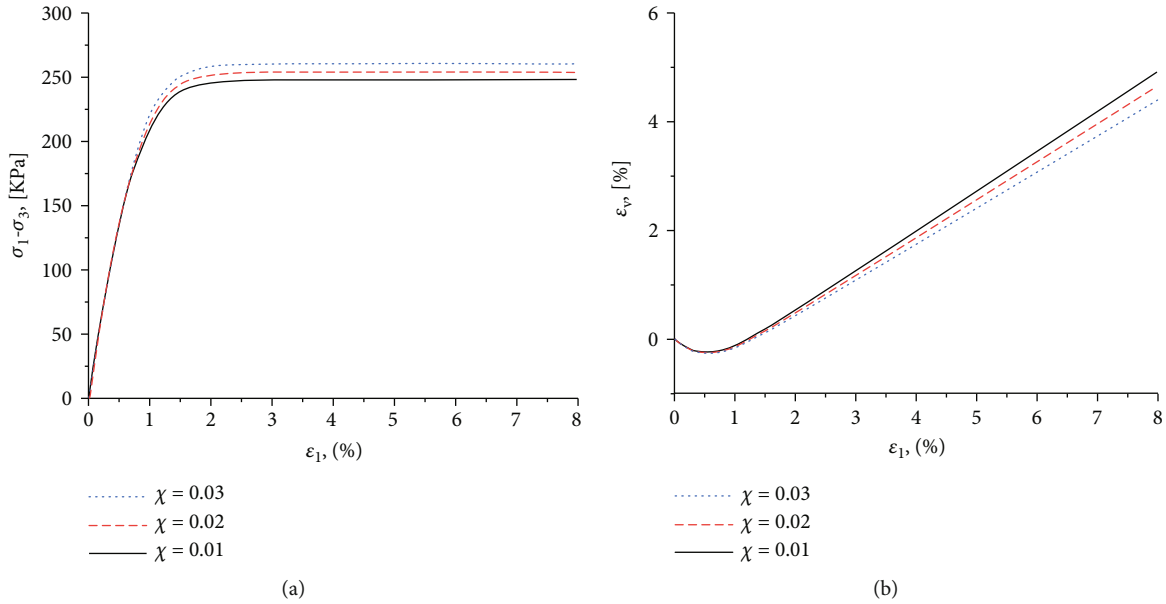

Figure 5: Simulation of triaxial tests for various material constant: (a) deviatoric stress vs. axial strain; (b) volumetric strain vs. axial strain.

follows:

$$\{\mathbf{M}\} = [\mathbf{B}]\{\mathbf{N}\} = \begin{bmatrix} \alpha & 0 & 0 & 0 & 0 & 0 \\ 0 & \beta & 0 & 0 & 0 & 0 \\ 0 & 0 & \beta & 0 & 0 & 0 \\ 0 & 0 & 0 & \gamma & 0 & 0 \\ 0 & 0 & 0 & 0 & \gamma & 0 \\ 0 & 0 & 0 & 0 & 0 & \beta \end{bmatrix} \begin{bmatrix} N_{11} \\ N_{22} \\ N_{33} \\ N_{23} \\ N_{13} \\ N_{12} \end{bmatrix}. \quad (5)$$

Referring to the tensorial function [45], Equation (5) can be rewritten as

$$\mathbf{M}(\mathbf{A}, \mathbf{N}) = (\alpha + \gamma - 2\beta) tr(\mathbf{AN})\mathbf{A} + \gamma\mathbf{N} + (\beta - \gamma)(\mathbf{AN} + \mathbf{NA}). \quad (6)$$

2.2. A Modified Model Considering the Relation between Fabric Tensor and Anisotropic Parameters. For sand and other typical granular materials in civil engineering, the influence of anisotropic microstructure (i.e., fabric) on mechanical characteristics, such as strength and deformation, is evident. Oda et al. [46] have performed a biaxial compression test on two kinds of sand to analyze the change of the fabric during deformation.

Figures 2 and 3 show the relation between stress ratio and anisotropy index as a function of $\theta = 0^\circ$ and $\theta = 60^\circ$, respectively. As shown in Figures 2 and 3, the measured stress ratios vary with the bedding angle, resulting in strength anisotropy (stress-induced anisotropy). Furthermore, from Figures 2 and 3, it is easily seen that the ratio N_1/N_2 is approximately proportional to the stress ratio. Therefore, they found that as the sample is loaded, the fabric evolves under the effect of external forces, resulting in stress-induced anisotropy.

Based on the above experimental results, Guo [47] considered that the fabric tensor component is proportional to the stress tensor component, by definition at

$$dF_{ij} = \chi \frac{d\sigma_{ij}}{p}, \quad (7)$$

where σ_{ij} and p are a stress tensor and mean principal stress, respectively. According to the condition of the triaxial compression test, the mean principal stress p can be defined as follows:

$$p = \frac{\sigma_1 + 2\sigma_3}{3}. \quad (8)$$

χ is evolution constant of the fabric that describes the stress-fabric relationship.

Osinov and Wu [32] assumed that the anisotropy is described using the vector a and the parameters (α, β, γ); the vector a gives the orientation of the bedding plane, while the parameters (α, β, γ) determine the degree of anisotropy. They proposed an anisotropic hypoplastic model by incorporating above two factors to predict the mechanical response of the anisotropic sand assuming the parameters (α, β, γ) are constant. But the assumption does not match the actual condition of the sand. This is the reason why the corresponding components of the stress rate vary during deformation, resulting in a change of the parameters (α, β, γ).

Therefore, we considered that the variation of parameters (α, β, γ) depends on the external loads in such a way that fabric evolution is occurred with external loading and assumed that the fabric tensor components are equivalent

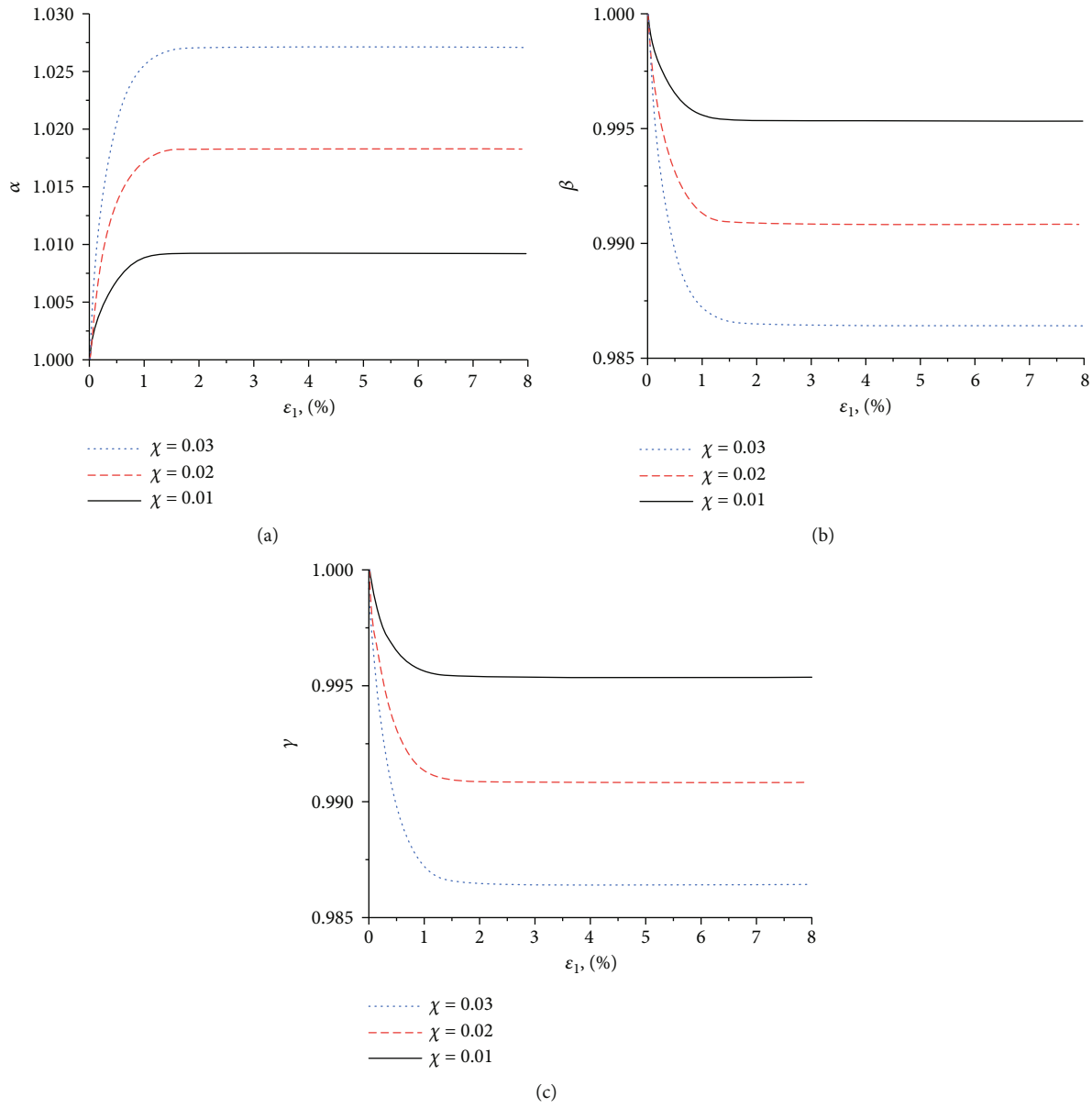

Figure 6: Changes of anisotropic parameters for various material constant: (a) α vs. axial strain; (b) β vs. axial strain; (c) γ vs. axial strain.

to the evolutions of anisotropic parameters.

$$dF_1 = d\alpha, dF_2 = d\beta, dF_3 = d\gamma. \tag{9}$$

Referring to Equation (9), three anisotropic parameters are defined as follows:

$$\alpha = \alpha_0 + d\alpha, \beta = \beta_0 + d\beta, \gamma = \gamma_0 + d\gamma, \tag{10}$$

where α_0, β_0, and γ_0 are initial values of three parameters.

Following Equations (1), (6), (7), (9), and (10), the modified model is established by considering the relation between the evolution of the fabric and anisotropic parameters under the external loading.

Table 1 shows the parameters of the modified anisotropic hypoplastic model for Karlsruhe sand.

As shown in Table 1, there are altogether eight parameters in the modified anisotropic hypoplastic model. Four parameters c_i $(i = 1, \cdots, 4)$ are dimensionless material parameters and these parameters can be obtained from triaxial compression test [8]. Three parameters α, β, and γ are anisotropic parameters, and these parameters determine the degree of anisotropy for the corresponding components of the stress rate, and the initial values of these parameters are all equal to 1, because the first stage of loading is isotropic consolidation of triaxial test. The second stage is compression of triaxial test, and the anisotropic parameters in this stage can be calculated from Equations (7), (9), and (10). The parameter χ is evolution constant of the fabric, and the parameter can be defined from Guo [47].

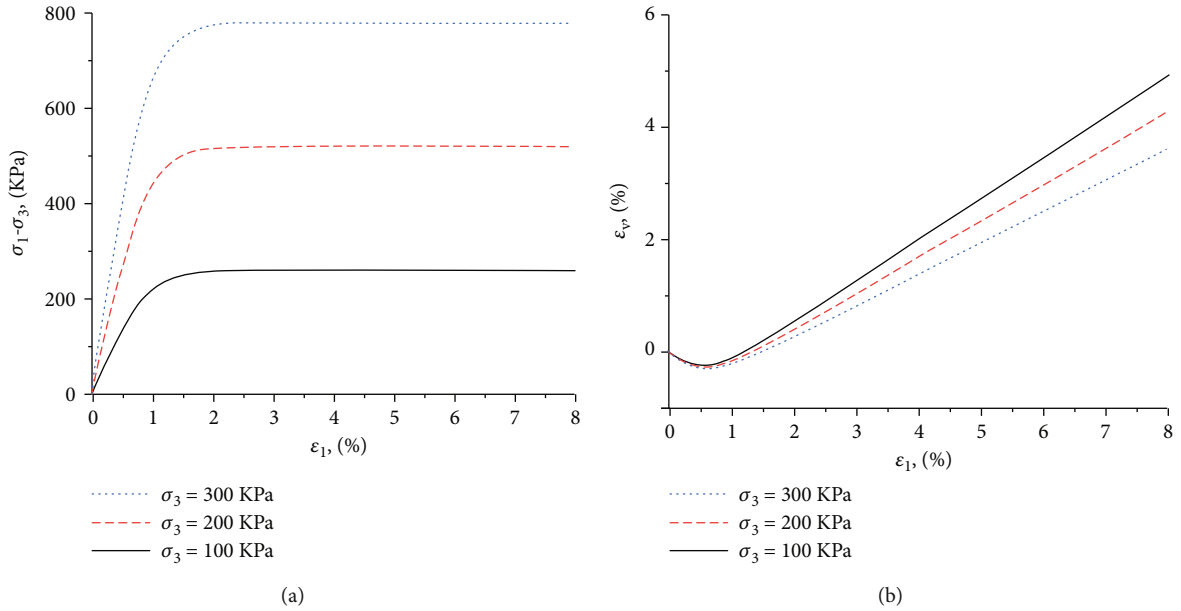

FIGURE 7: Simulation of triaxial tests for various confining pressure: (a) deviatoric stress vs. axial strain; (b) volumetric strain vs. axial strain.

3. Simulation Scheme

The improved model is used to simulate the triaxial compression test for Karlsruhe sand. The parameters for the Karlsruhe sand used in the simulation are listed in Table 1. The initial void ratio is $e_0 = 0.52$, and confining pressures σ_3 are 100, 200, and 300 KPa. Based on the following hypoplastic model proposed by Wu and Bauer [8], we proceed to consider anisotropic hypoplastic model.

$$\dot{\mathbf{T}} = c_1(\mathrm{tr}\mathbf{T})\mathbf{D} + c_2\frac{\mathrm{tr}(\mathbf{TD})\mathbf{T}}{\mathrm{tr}\mathbf{T}} + \left(c_3\frac{\mathbf{T}^2}{\mathrm{tr}\mathbf{T}} + c_4\frac{\mathbf{T}_d^2}{\mathrm{tr}\mathbf{T}}\right)\|\mathbf{D}\|. \quad (11)$$

The deviatoric stress tensor in Equation (11) is given by $\mathbf{T}_d = \mathbf{T} - 1/3(\mathrm{tr}\mathbf{T})\mathbf{1}$ ($\mathbf{1}$ is the second-order unity tensor). In a triaxial compression test for anisotropic sand, the governing differential equations are defined as follows:

$$\begin{aligned}\dot{\sigma}_1 &= c_1(\sigma_1 + 2\sigma_3)\dot{\varepsilon}_1 + c_2\frac{\sigma_1\dot{\varepsilon}_1 + \sigma_3(\dot{\varepsilon}_2 + \dot{\varepsilon}_3)}{\sigma_1 + 2\sigma_3}\sigma_1 \\ &+\left\{(\alpha + \gamma - 2\beta)\left[c_3\left(\sigma_1^2\cos^2\theta + \sigma_2^2\sin^2\theta\right) + \frac{1}{9}c_4\left((\sigma_1 - \sigma_3)^2\left(1 + 3\cos^2\theta\right)\right)\right]\cos^2\theta\right. \\ &\left.+\gamma\left[c_3\sigma_1^2 + \frac{4}{9}c_4(\sigma_1 - \sigma_3)^2\right] + (\beta - \gamma)\left[2c_3\sigma_1^2\cos^2\theta + \frac{8}{9}c_4\cos^2\theta(\sigma_1 - \sigma_3)^2\right]\right\}B,\end{aligned} \quad (12)$$

$$\begin{aligned}\dot{\sigma}_2 &= c_1(\sigma_1 + 2\sigma_3)\dot{\varepsilon}_2 + c_2\frac{\sigma_1\dot{\varepsilon}_1 + \sigma_3(\dot{\varepsilon}_2 + \dot{\varepsilon}_3)}{\sigma_1 + 2\sigma_3}\sigma_2 \\ &+\left\{(\alpha + \gamma - 2\beta)\left[c_3\left(\sigma_1^2\cos^2\theta + \sigma_2^2\sin^2\theta\right) + \frac{1}{9}c_4\left((\sigma_1 - \sigma_3)^2\left(1 + 3\cos^2\theta\right)\right)\right]\sin^2\theta\right. \\ &\left.+\gamma\left[c_3\sigma_2^2 + \frac{1}{9}c_4(\sigma_1 - \sigma_3)^2\right] + (\beta - \gamma)\left[2c_3\sigma_2^2\sin^2\theta + \frac{2}{9}c_4\sin^2\theta(\sigma_1 - \sigma_3)^2\right]\right\}B,\end{aligned} \quad (13)$$

$$\begin{aligned}\dot{\sigma}_3 &= c_1(\sigma_1 + 2\sigma_3)\dot{\varepsilon}_3 + c_2\frac{\sigma_1\dot{\varepsilon}_1 + \sigma_3(\dot{\varepsilon}_2 + \dot{\varepsilon}_3)}{\sigma_1 + 2\sigma_3}\sigma_3 \\ &+\left\{\gamma\left[c_3\sigma_3^2 + \frac{1}{9}c_4(\sigma_1 - \sigma_3)^2\right]\right\}B,\end{aligned} \quad (14)$$

$$\begin{aligned}\dot{\sigma}_{12} &= c_1(\sigma_1 + 2\sigma_3)\dot{\varepsilon}_{12} + \left\{(2\beta - \alpha - \gamma)\left[c_3\left(\sigma_1^2\cos^2\theta + \sigma_2^2\sin^2\theta\right)\right.\right. \\ &\left.+\frac{1}{9}c_4\left((\sigma_1 - \sigma_3)^2\left(1 + 3\cos^2\theta\right)\right)\right]\sin\theta\cos\theta \\ &\left.+(\gamma - \beta)\left[c_3\left(\sigma_1^2 + \sigma_3^2\right)\sin\theta\cos\theta + \frac{5}{9}c_4(\sigma_1 - \sigma_3)^2\sin\theta\cos\theta\right]\right\}B,\end{aligned} \quad (15)$$

$$\dot{\sigma}_{13} = c_1(\sigma_1 + 2\sigma_3)\dot{\varepsilon}_{13}, \quad (16)$$

$$\dot{\sigma}_{23} = c_1(\sigma_1 + 2\sigma_3)\dot{\varepsilon}_{23}, \quad (17)$$

where

$$B = \frac{\sqrt{\dot{\varepsilon}_1^2 + \dot{\varepsilon}_2^2 + \dot{\varepsilon}_3^2 + 2\dot{\varepsilon}_{12}^2 + 2\dot{\varepsilon}_{13}^2 + 2\dot{\varepsilon}_{23}^2}}{\sigma_1 + 2\sigma_3}. \quad (18)$$

A MATLAB code was created to simulate the triaxial test using a four parameter-anisotropic hypoplastic model. Using Equations ((12)–(17)), the code computes the corresponding stress-strain and volume change for every time step. Figure 4 shows the MATLAB code's operation flow. The four material parameters c_1, c_2, c_3, and c_4 are input in the (input material constant) step. In a triaxial compression test ($\sigma_1 > \sigma_2 = \sigma_3$), the confining pressure is constant, so $\dot{\sigma}_2 = \dot{\sigma}_3 = 0$. The bedding angles θ are 0°, 30°, 60°, and 90°. Initial values of three anisotropic parameters are given by $\alpha = 1$, $\beta = 1$, and $\gamma = 1$, respectively. Even more, the initial conditions are entered in the (initial condition) step. The axial strain increment $\dot{\varepsilon}_1$ is entered in the (external force condition) step. All

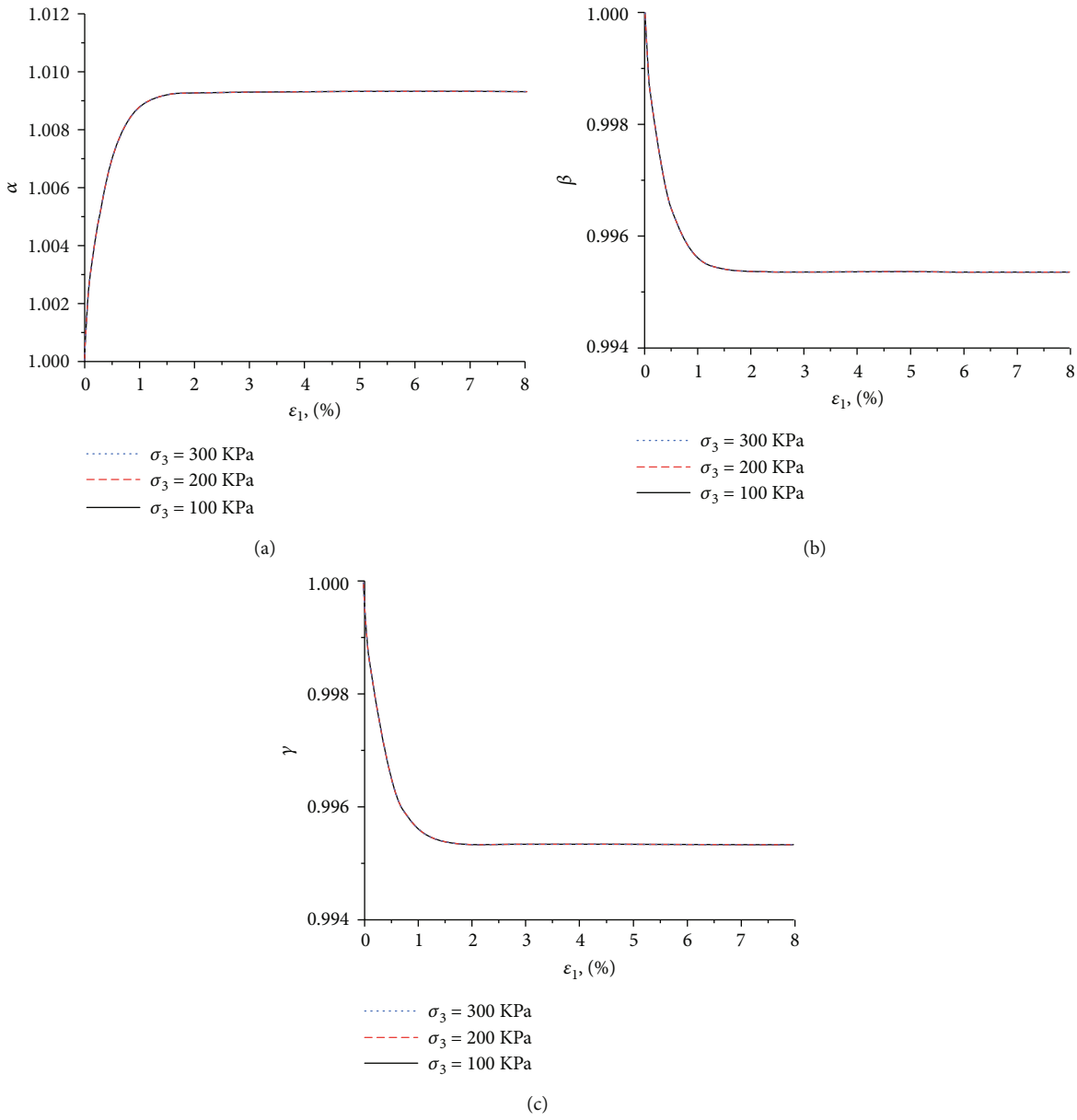

Figure 8: Changes of anisotropic parameters for various confining pressure: (a) α vs. axial strain; (b) β vs. axial strain; (c) γ vs. axial strain.

calculations are performed by six functions mentioned above (Equations ((12)–(17))): five auxiliary functions and one main function. In each time step, the strain increments $(\dot{\varepsilon}_2, \dot{\varepsilon}_3, \dot{\varepsilon}_{12}, \dot{\varepsilon}_{13}, \dot{\varepsilon}_{23})$ are calculated from the (auxiliary functions) step. The obtained strain rates are fed into the (main function) step to get the axial stress rate and the anisotropic factor rates. The auxiliary functions are Equations ((13)–(17)), and the main function is Equation (12). Following this, the axial stress and anisotropic factors are changed. This process is iterated until the total axial strain meets the requirements. When the total axial strain satisfies the requirements, it is gone to the (result analysis) step, and the mechanical responses are analyzed.

4. Simulation Results

The improved model is used to simulate the influences of the material constant χ, confining pressure σ_3, and bedding angle θ on the mechanical response of anisotropic soil.

4.1. Effect of Material Constant χ on the Mechanical Response of Anisotropic Soil. The modified model is used to simulate the numerical triaxial test for Karlsruhe sand. Figure 5 shows the relations between the deviatoric stress and axial strain and volumetric strain and axial strain according to the change of material constant χ. The confining pressure σ_3 is equal to 100 KPa, and bedding angle θ is equal to 0°. As shown in Figure 5, an increase in material

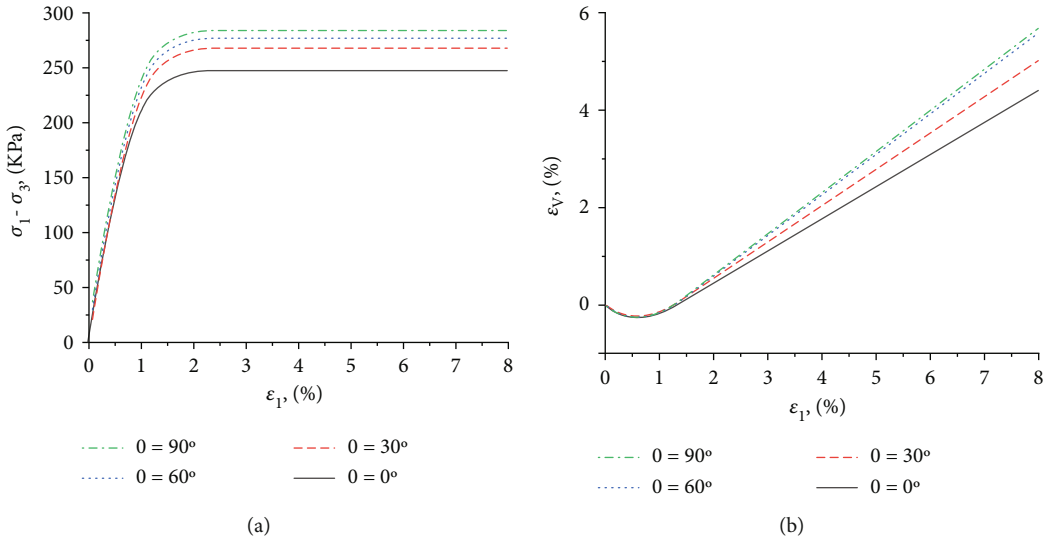

Figure 9: Simulation of triaxial tests for various bedding angle: (a) deviatoric stress vs. axial strain; (b) volumetric strain vs. axial strain.

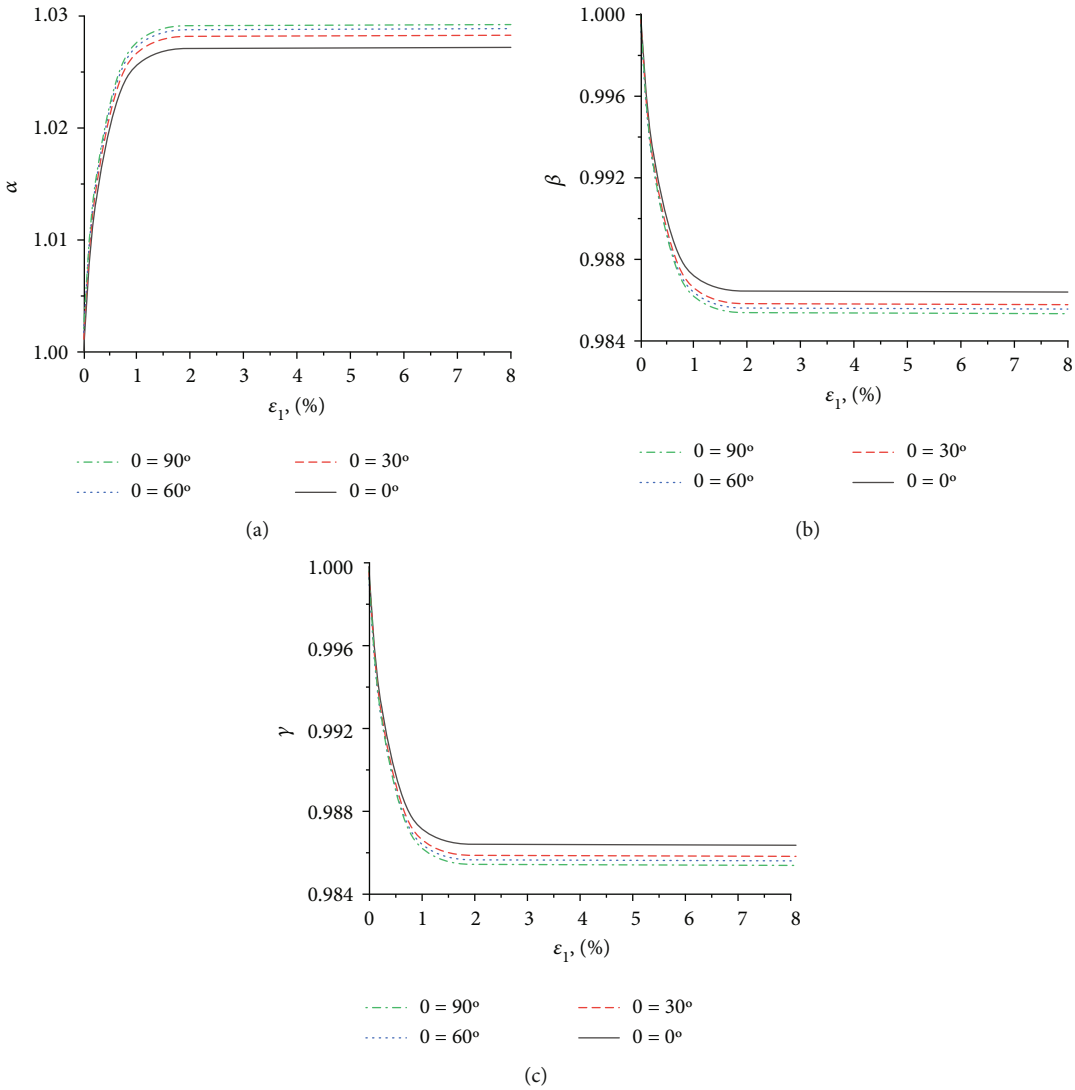

Figure 10: Changes of anisotropic parameters for various bedding angle: (a) α vs. axial strain; (b) β vs. axial strain; (c) γ vs. axial strain.

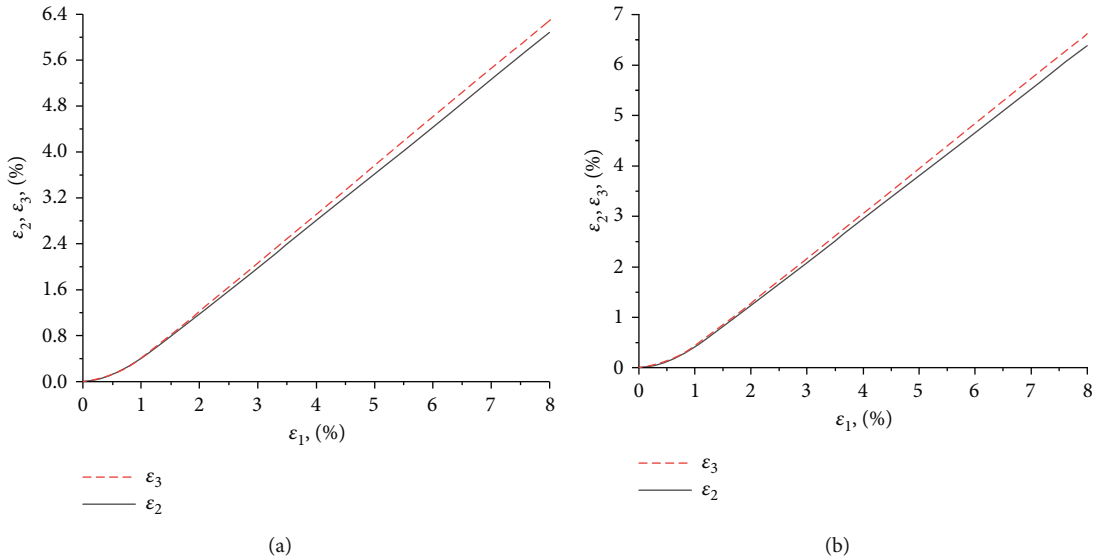

Figure 11: Principal strains during triaxial compression (χ =0.03, σ_3 =200 KPa): (a) θ =30°; (b) θ =60°.

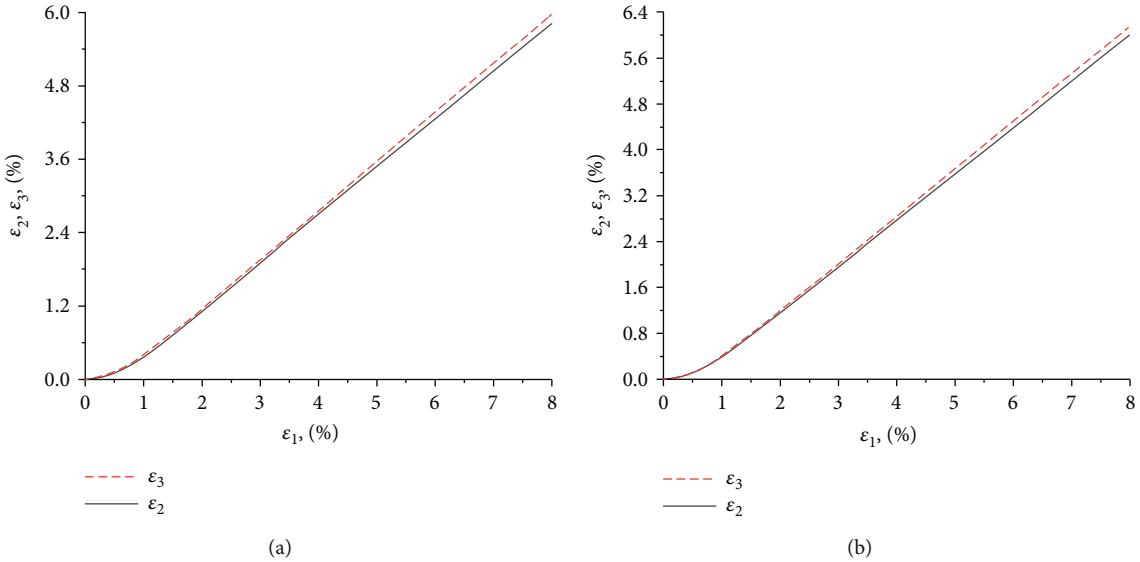

Figure 12: Principal strains during triaxial compression (χ =0.02, σ_3 =300 KPa): (a) θ =30°; (b) θ =60°.

constant χ relatively causes increase in deviatoric stress. This is the reason why the material constant affected the anisotropic parameters, which results in the difference of response of deviatoric stress. Figure 6 shows the change of anisotropic parameters according to the material parameters.

From Figure 6, it is found that, with the augmentation of material constant χ, the change of parameter α increases, and the variations of parameters β and γ decrease. With the material parameter constant, α increases initially until to reach a constant value, and then keep a constant. But comparing with α, parameters β and γ firstly decrease to reach a constant value, and then keep the same. This reflects the mechanical response of anisotropic soil.

4.2. Effect of Confining Pressure σ_3 on the Mechanical Response of Anisotropic Soil. The simulation results of triaxial tests according to various confining pressure are shown in Figure 7. The bedding angle θ and the material constant χ are equal to 0° and 0.01, respectively. As shown in Figure 7, it is found that the new improved model can well predict the response of confining pressure on the mechanical property of anisotropic soil.

The changes of parameters α, β, and γ are presented in Figure 8. The variation of the anisotropic parameters was similar to that of material constant χ under constant confining pressure. But as noted in Figure 8, for all cases of various confining pressure, changes of anisotropic parameters were all same, that is, there is no effects of confining pressure on the variation of anisotropic parameters. As a result, it can be seen that external force has greater effect on the changes of anisotropic parameters than confining pressure.

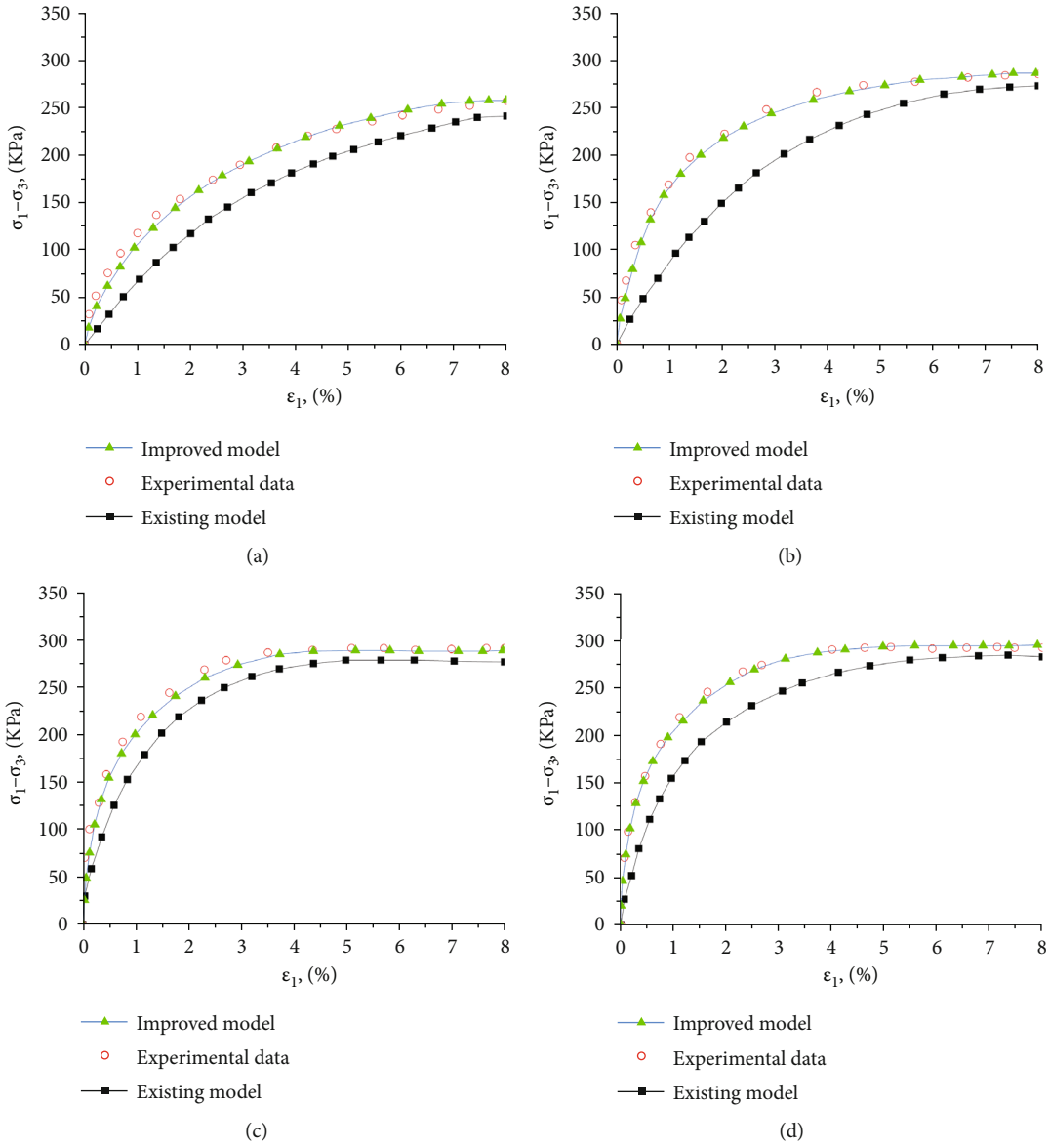

Figure 13: Comparison of two models with the experimental data by Oda [49]: (a) θ =0°; (b) θ =30°; (c) θ =60°; (d) θ =90°.

4.3. Effect of Bedding Angle θ on the Mechanical Response of Anisotropic Soil. Figure 9 shows the response of bedding angle on the mechanical property of anisotropic soil, and it can be noticed that the deviatoric stress increases as the bedding angle rises. The confining pressure σ_3 and the material constant χ are equal to 100 KPa and 0.03, respectively. For all the values of bedding angles, the volumetric strain-axial strain curve exhibits the same trend; volumetric strains firstly contract and then dilatate. The changes of anisotropic parameters are shown in Figure 10. With increase in bedding angles, changes of anisotropic parameter α rises, while β and γ decrease. Under the condition of constant bedding angle, the anisotropic parameter α firstly increases to reach maximum value, and then keeps that value. It is found that the change of anisotropic parameter α reflects the mechanical response of bedding angle on the anisotropic soil. In contrast of parameter α, anisotropic parameters β and γ initially decrease to minimum value, and subsequently do not change.

In general, anisotropic soil exhibits the nonaxisymmetric deformation to the loading axes according to the bedding angles [48]. Therefore, the modified model is used to verify the nonaxisymmetric deformation. Figures 11 and 12 show the relations between the axial strain and radial strains according to the bedding angles in two cases (first case: χ =0.03, σ_3 =200 KPa; second case: χ =0.02, σ_3 =300 KPa), respectively.

As shown in Figures 11 and 12, in two cases, the values for the radial strains all differ from each other, that is, the mechanical response of bedding angles on the anisotropic soil exhibits the nonaxisymmetric deformation about the loading axes.

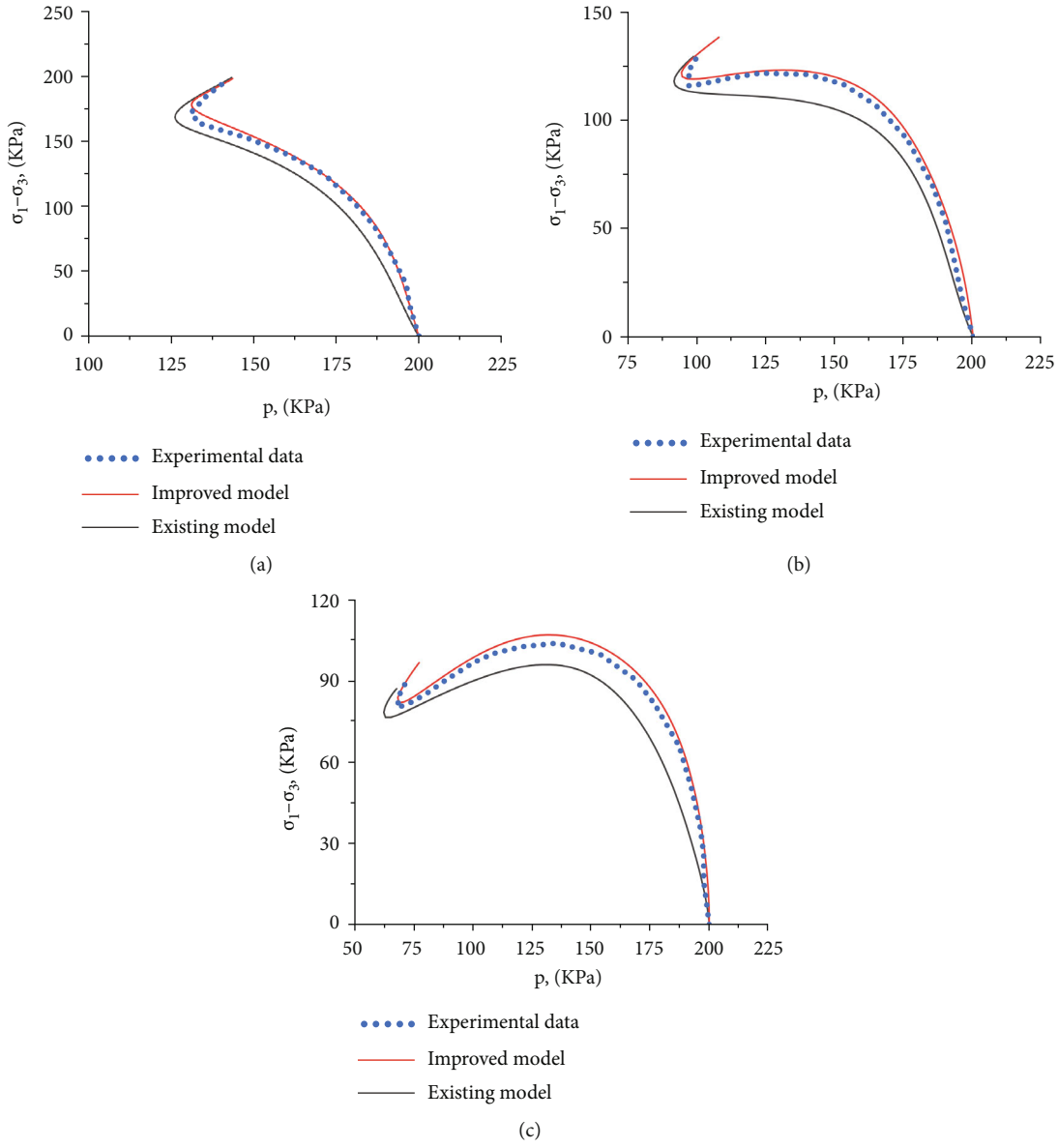

Figure 14: Comparison of two models and the experimental results by Uthayakumar and Vaid [50] for undrained triaxial tests (stress path response): (a) $\theta=0^{\circ}$; (b) $\theta=30^{\circ}$; (c) $\theta=60^{\circ}$.

4.4. Comparison with the Existing Model and Experimental Data. Wu [28] proposed the anisotropic hypoplastic model by incorporating anisotropic operator into the nonlinear part of constitutive model. But this model was used to simulate the mechanical property of anisotropic soil under the condition of constant anisotropic parameters. The new improved model was based on the same model from Wu [28] but was developed considering the change of anisotropic parameters. Therefore, the improved model was validated by comparing simulation results with existing model proposed from Wu [28].

The first verification is done by the experimental data conducted from Oda [49]. Wu [28] used the following constants for numerical simulations: $\alpha=0.9$, $\beta=1.0$, and $\gamma=1.1$. Oda [49] has conducted a drained triaxial compression test with confining pressure of 100 KPa and strain rate of 0.2%/min and analyzed the mechanical property of anisotropic soil. The bedding angles were 0°, 30°, 60°, and 90°. Figure 13 shows the comparison of two models with experimental data.

As shown in Figures 13(a–d), in all cases, by comparing simulation results with the experimental data of the drained triaxial compression test, it is found that the new improved model shows a significantly better agreement with experimental data than the existing model. That is the reason why the modified model can be used for modeling the mechanical property of anisotropic soil by considering the change of anisotropic parameters according to external loading, while the existing model was based on the condition of constant anisotropic parameters. It is then proven that the

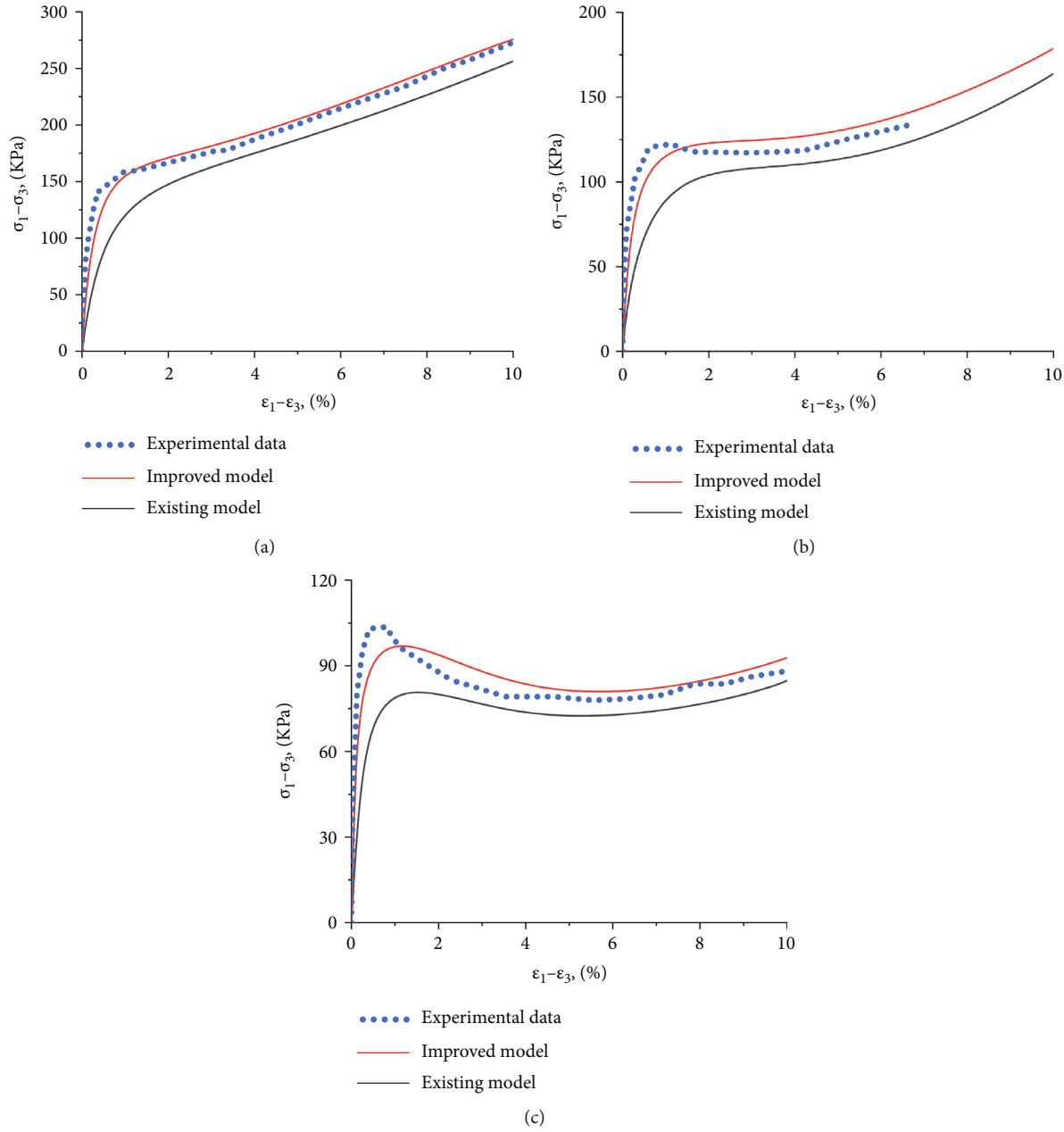

FIGURE 15: Comparison of two models and the experimental results by Uthayakumar and Vaid [50] for undrained triaxial tests (deviator stress-shear strain): (a) $\theta = 0^{\circ}$; (b) $\theta = 30^{\circ}$; (c) $\theta = 60^{\circ}$.

improved model provides good predictions for the response of anisotropic soil.

The last verification is done by using experimental results from Uthayakumar and Vaid [50]. They have conducted the undrained triaxial tests on Fraser River sand in a hollow cylinder torsional shear device. Fraser River sand was dry-deposited according to the bedding angles. The confining pressure was 200 KPa, and the bedding angles were 0°, 30°, and 60°. All the samples have the same relative density of Dr = 30%.

Figures 14 and 15 show the simulation results of stress path and deviator stress-shear strain relation for undrained triaxial tests with the bedding angles, respectively. From Figures 14 and 15, it can be found that the two models can adequately predict the undrained behavior of anisotropic sand. In particular, the simulation result of the improved model agrees better with the experimental data than that of the existing model.

5. Conclusions

The hallmark of the improved model lies in considering the relation between the fabric tensor and anisotropic parameters. The new improved model is extended by a new anisotropic parameters. The anisotropic parameters are defined

in such a way that fabric tensor was changed according to external loading.

The modified model has been evaluated by analyzing the effects of the material constant, bedding angle, and confining pressure on the mechanical property of anisotropic soil. The results show that the improved model can well predict the response of anisotropic soil. In addition, the new improved model reflects the nonaxisymmetric deformation to the loading axes in the anisotropic soil, according to the bedding angles.

The modified model was compared to existing model proposed by Wu [28] and experimental data conducted by Oda [49] and Uthayakumar and Vaid [50]. The simulation results of the improved model are closer to the experimental data than existing model. The modified model has advantage to predict the actual response of anisotropic soil. In the future, it is paid special attention to use the improved model for modeling boundary value problems under cyclic loading and develop the anisotropic hypoplastic model within the anisotropic critical state framework.

Data Availability

All data are available from the corresponding author upon request.

Conflicts of Interest

The authors declare that there are no conflicts of interest on the publication of this paper.

Acknowledgments

The authors gratefully acknowledge the financial support provided by the Beijing Municipal Natural Science Foundation [No. 8222020].

References

[1] Y. F. Dafalias, M. T. Manzari, and M. Akaishi, "A simple anisotropic clay plasticity model," *Mechanics Research Communications*, vol. 29, no. 4, pp. 241–245, 2002.

[2] D. A. Sun, H. Matsuoka, Y. P. Yao, and H. Ishii, "An anisotropic hardening elastoplastic model for clays and sands and its application to FE analysis," *Computers and Geotechnics*, vol. 31, no. 1, pp. 37–46, 2004.

[3] J. H. Jiang and H. I. Ling, "A framework of an anisotropic elastoplastic model for clays," *Mechanics Research Communications*, vol. 37, no. 4, pp. 394–398, 2010.

[4] N. Sivasithamparam and J. Castro, "An anisotropic elastoplastic model for soft clays based on logarithmic contractancy," *International Journal for Numerical and Analytical Methods in Geomechanics*, vol. 40, no. 4, pp. 596–621, 2016.

[5] N. Hu, H. S. Yu, D. S. Yang, and P. Z. Zhuang, "Constitutive modelling of granular materials using a contact normal-based fabric tensor," *Acta Geotechnica*, vol. 15, no. 5, pp. 1125–1151, 2020.

[6] T. L. Rong, C. Guan, K. L. Liu, S. Heng, W. L. Shen, and R. Y. Mou, "A statistical damage constitutive model of anisotropic rock: development and validation," *Geofluids*, vol. 2021, Article ID 6307895, 16 pages, 2021.

[7] D. Kolymbas, "An outline of hypoplasticity," *Archive of Applied Mechanics*, vol. 61, no. 3, pp. 143–151, 1991.

[8] W. Wu and E. Bauer, "A simple hypoplastic constitutive model for sand," *International Journal for Numerical and Analytical Methods in Geomechanics*, vol. 18, no. 12, pp. 833–862, 1994.

[9] W. Wu, J. Lin, and X. T. Wang, "A basic hypoplastic constitutive model for sand," *Acta Geotechnica*, vol. 12, no. 6, pp. 1373–1382, 2017.

[10] G. Gudehus, "A comprehensive constitutive equation for granular materials," *Soils and Foundations*, vol. 36, no. 1, pp. 1–12, 1996.

[11] E. Bauer, "Calibration of a comprehensive hypoplastic model for granular materials," *Soils and Foundations*, vol. 36, no. 1, pp. 13–26, 1996.

[12] P. A. Von Wolffersdorff, "A hypoplastic relation for granular materials with a predefined limit state surface," *Mechanics of Cohesive-Frictional Materials*, vol. 1, no. 3, pp. 251–271, 1996.

[13] G. Zhang, W. Wu, and J. M. Zhang, "Hypoplasticity damage model of coarse-grained soils," *Journal-Tsinghua University*, vol. 46, no. 6, pp. 793–796, 2006.

[14] A. Niemunis and I. Herle, "Hypoplastic model for cohesionless soils with elastic strain range," *Mechanics of Cohesive-frictional Materials*, vol. 2, no. 4, pp. 279–299, 1997.

[15] B. L. Xiong and C. J. Lu, "Amelioration of Wolffersdorff hypoplastic constitutive model considering intergranular strain tensor," in *Presented at the 3rd International Conference on Civil, Architectural and Hydraulic Engineering (ICCAHE)*, vol. 638-640, pp. 355–359, Hangzhou, PEOPLES R CHINA, 2014.

[16] B. Xiang, Z. L. Zhang, and S. C. Chi, "An improved hypoplastic constitutive model of rockfill considering effect of stress path," *Journal of Central South University of Technology*, vol. 16, no. 6, pp. 1006–1013, 2009.

[17] W. Fuentes, T. Triantafyllidis, and A. Lizcano, "Hypoplastic model for sands with loading surface," *Acta Geotechnica*, vol. 7, no. 3, pp. 177–192, 2012.

[18] N. T. V. Phuong, A. Rohe, R. B. J. Brinkgreve, and A. F. van Tol, "Hypoplastic model for crushable sand," *Soils and Foundations*, vol. 58, no. 3, pp. 615–626, 2018.

[19] J. Liu, S. Wang, M. J. Jiang, and W. Wu, "A state-dependent hypoplastic model for methane hydrate-bearing sands," *Acta Geotechnica*, vol. 16, no. 1, pp. 77–91, 2021.

[20] W. X. Huang, W. Wu, D. A. Sun, and S. Sloan, "A simple hypoplastic model for normally consolidated clay," *Acta Geotechnica*, vol. 1, no. 1, pp. 15–27, 2006.

[21] D. Masin and I. Herle, "Improvement of a hypoplastic model to predict clay behaviour under undrained conditions," *Acta Geotechnica*, vol. 2, no. 4, pp. 261–268, 2007.

[22] D. Masin and N. Khalili, "A hypoplastic model for mechanical response of unsaturated soils," *International Journal for Numerical and Analytical Methods in Geomechanics*, vol. 32, no. 15, pp. 1903–1926, 2008.

[23] Y. T. Ding, W. X. Huang, D. C. Sheng, and S. W. Sloan, "Numerical study on finite element implementation of hypoplastic models," *Computers and Geotechnics*, vol. 68, pp. 78–90, 2015.

[24] S. Wang and W. Wu, "Validation of a simple hypoplastic constitutive model for overconsolidated clays," *Acta Geotechnica*, vol. 16, no. 1, pp. 31–41, 2021.

[25] S. Wang and W. Wu, "A simple hypoplastic model for overconsolidated clays," *Acta Geotechnica*, vol. 16, no. 1, pp. 21–29, 2021.

[26] S. Wang, W. Wu, D. C. Zhang, and J. R. Kim, "Extension of a basic hypoplastic model for overconsolidated clays," *Computers and Geotechnics*, vol. 123, p. 103486, 2020.

[27] J. Jerman and D. Masin, "Evaluation of hypoplastic model for soft clays by modelling of Nicoll highway case history," *Computers and Geotechnics*, vol. 134, p. 104053, 2021.

[28] W. Wu, "Rational approach to anisotropy of sand," *International Journal for Numerical and Analytical Methods in Geomechanics*, vol. 22, no. 11, pp. 921–940, 1998.

[29] A. Niemunis, "Anisotropic effects in hypoplasticity," in *Presented at the 3rd International Symposium on Deformation Characteristics of Geomaterials*, Lyon, France, 2003.

[30] E. Bauer, W. X. Huang, and W. Wu, "Investigations of shear banding in an anisotropic hypoplastic material," *International Journal of Solids and Structures*, vol. 41, no. 21, pp. 5903–5919, 2004.

[31] J. Tejchman, "Investigations of shear localization in granular bodies within an anisotropic micro-polar hypoplasticity," *Archives of Hydro-Engineering and Environmental Mechanics*, vol. 52, no. 4, pp. 351–371, 2005.

[32] V. A. Osinov and W. Wu, "Simple shear in sand with an anisotropic hypoplastic model," *Geomechanics and Geoengineering*, vol. 1, no. 1, pp. 43–50, 2006.

[33] J. Tejchman and W. Wu, "Modeling of textural anisotropy in granular materials with stochastic micro- polar hypoplasticity," *International Journal of Non-Linear Mechanics*, vol. 42, no. 6, pp. 882–894, 2007.

[34] B. Weingartner, V. A. Osinov, and W. Wu, "Effect of inherent anisotropy on acceleration wave speeds in hypoplasticity," *International Journal of Engineering Science*, vol. 46, no. 3, pp. 286–292, 2008.

[35] C. Herrera and A. Lizcano, "A hypoplastic sand model taking into account fabric," *GeoFlorida 2010: Advances in Analysis, Modeling and Design*, 2010.

[36] D. Masin, "Clay hypoplasticity model including stiffness anisotropy," *Geotechnique*, vol. 64, no. 3, pp. 232–238, 2014.

[37] J. Jerman and D. Mašín, "Hypoplastic and viscohypoplastic models for soft clays with strength anisotropy," *International Journal for Numerical and Analytical Methods in Geomechanics*, vol. 44, no. 10, pp. 1396–1416, 2020.

[38] M. Tafili and T. Triantafyllidis, "A simple hypoplastic model with loading surface accounting for viscous and fabric effects of clays," *International Journal for Numerical and Analytical Methods in Geomechanics*, vol. 44, no. 16, pp. 2189–2215, 2020.

[39] Z. X. Yang, D. Liao, and T. T. Xu, "A hypoplastic model for granular soils incorporating anisotropic critical state theory," *International Journal for Numerical and Analytical Methods in Geomechanics*, vol. 44, no. 6, pp. 723–748, 2020.

[40] W. Fuentes, D. Masin, and J. Duque, "Constitutive model for monotonic and cyclic loading on anisotropic clays," *Geotechnique*, vol. 71, no. 8, pp. 657–673, 2021.

[41] D. Liao and Z. X. Yang, "Hypoplastic modeling of anisotropic sand behavior accounting for fabric evolution under monotonic and cyclic loading," *Acta Geotechnica*, vol. 16, no. 7, pp. 2003–2029, 2021.

[42] D. Liao and Z. X. Yang, "Non-coaxial hypoplastic model for sand with evolving fabric anisotropy including non-proportional loading," *International Journal for Numerical and Analytical Methods in Geomechanics*, vol. 45, no. 16, pp. 2433–2463, 2021.

[43] D. Liao and Z. X. Yang, "Hypoplastic model for sand under multidirectional shearing conditions considering fabric change effect," *Soil Dynamics and Earthquake Engineering*, vol. 155, p. 107168, 2022.

[44] J. Duque, M. Tafili, G. Seidalinov, D. Mašín, and W. Fuentes, "Inspection of four advanced constitutive models for fine-grained soils under monotonic and cyclic loading," *Acta Geotechnica*, vol. 17, pp. 4395–4418, 2022.

[45] J. P. Boehler and A. Sawczuk, "On yielding of oriented solids," *Acta Mechanica*, vol. 27, no. 1-4, pp. 185–204, 1977.

[46] M. Oda, S. Nemat-Nasser, and J. Konishi, "Stress-induced anisotropy in granular masses," *Soils and Foundations*, vol. 25, no. 3, pp. 85–97, 1985.

[47] P. J. Guo, "Modelling granular materials with respect to stress-dilatancy and fabric-a fundamental approach," University of Calgary, 2000.

[48] Y. Togashi, M. Kikumoto, K. Tani, K. Hosoda, and K. Ogawa, "Detection of deformation anisotropy of tuff by a single triaxial test on a single specimen," *International Journal of Rock Mechanics and Mining Sciences*, vol. 108, pp. 23–36, 2018.

[49] M. Oda, "Initial fabrics and their relations to mechanical properties of granular material," *Soils and Foundations*, vol. 12, no. 1, pp. 17–36, 1972.

[50] M. Uthayakumar and Y. P. Vaid, "Static liquefaction of sands under multiaxial loading," *Canadian Geotechnical Journal*, vol. 35, no. 2, pp. 273–283, 1998.